SSCL-N-839

Soft X-Ray Reflectivity Measurements for Technical Surfaces

Q. Jiang and A. Maschke

Superconducting Super Collider Laboratory*
2550 Beckleymeade Ave.
Dallas, TX 75237

P. Lippel, A. Weiss, A. Koymen, S. Yang, and S. Erichsrud

University of Texas at Arlington
Department of Physics
Box 19059
Arlington, TX 76019

December 1993

*Operated by the Universities Research Association, Inc., for the U.S. Department of Energy under Contract No. DE-AC35-89ER40486.

Soft X-Ray Reflectivity Measurements for Technical Surfaces

Q. T. Jiang[†], P. Lippel[‡], A. Weiss[‡], A. Koymen[‡], S. Yang[‡], S. Erichsrud[‡] and A. Maschke[†]

[†]Superconducting Super Collider Laboratory, MS 1046
2550 Beckleymeade Ave. Dallas, TX 75237

[‡]Department of Physics, Box 19059
University of Texas at Arlington, Arlington, TX 76019

Abstract

Synchrotron radiation has become an important design consideration for high energy particle accelerators, especially for the next generation proton colliders such as American Superconducting Super Collider (SSC) and European CERN Large Hadron Collider (LHC). In this paper, we report measurements of soft X-ray surface reflectivity of proton collider beam tube candidates, using synchrotron radiation source at Brookhaven National Lab, U-16A beam line. Our results show that by changing the surface rms roughness height from ~1 μm to ~10 μm, surface specular reflectivity is altered by two orders of magnitude. The total reflections for smooth and rough surfaces are also quite different, with ~90% for the smooth one and ~10% for the rough. The refractive indices found from these surfaces are different from the bulk values and shift toward oxide values.

I. Introduction

Modern high energy accelerator storage ring requires residual gas loads in the 10^{-10} torr range. Low pressures are necessary so that the particle beam can circulate for many hours without undue loss due to Coulomb and nuclear scattering from residual gas molecules.

In designs for next generation proton accelerators, protons will be accelerated to and stored at as high as many TeV's, to achieve the required beam bending and make the beam circulate, strong magnetic fields have to be employed. The dipole strengths need to be as high as 6 to 9 Tesla, which require superconducting magnets operate around liquid helium temperature (4.2° K) or lower. Under this condition, most of the residual gas will be frozen on the beam tube walls. In operation, the relativistic protons, when accelerated in the bending magnets, will emit synchrotron radiation with critical energies of 286 eV and 51.2 eV, and photon flux of $1.0*10^{16}$ /meter-second and $1.6*10^{17}$ /meter-second for SSC[1] and LHC[2] respectively. Presence of considerable synchrotron radiation which can cause stimulated desorption from the beam tube walls represents a potential problem.[3, 4]

An additional challenge is presented by the fact that due to the very limited temperature tolerance of the magnets, the ion storage ring is not bakable. The baseline design of the SSC vacuum system relies on cryotrapping at the tube walls to attain UHV, while LHC relies on separate liner inside its storage ring. Thus desorbed molecules are not actually removed from the vacuum system but are merely redistributed along the beam pipe. If a sufficient quantity of molecules (such as H_2) accumulates in weakly bound states (like physisorption states), the pressure could quickly rise to unacceptable values.

Measurements were carried out in our lab which were aimed at understanding the factor involved in determining the vacuum conditions for the next generation particle accelerators and at finding suitable beam tube materials. This includes measurements of photon and electron stimulated desorption coefficients, photon and electron reflection coefficients, photoelectron production cross sections, and angular distribution of desorbed species (particularly H_2) for candidate beam-tube materials. The goal of our experiments was to characterize beam-tube candidates in order to find the optimum working condition for collider

beam tube materials. Details of our *in-situ* experimental plan at cryogenic temperatures can be found elsewhere.[3]

In understanding photon induced desorption and relevant issues, it is important to understand how photons are distributed through reflection in the beam tube. The majority of the previous reflectivity measurements have been performed on mirror like surfaces. Measurements on rough surfaces like accelerator storage ring walls, where surface rms roughness height is much larger than photon wave length, are rare. The purpose of this paper is to present our experimental measurements on the soft X-ray optical behaviors for accelerator beam tube candidates.

The materials studied in this paper, consists of stainless steel tube section electroplated on the inside with 100 microns of copper. The layer of high conducting materil is necessary in order to reduce image current wall losses that could create unacceptable heat loads as well as lead to beam instabilities. The base line design of the SSC is for 100 microns electroplated copper. The diameter of the beam-tube is around 3.8 cm, which implies a 0.26 cm^{-1} curvature along the transverse direction. From the macroscopic point of view, the surfaces we are dealing with are by no means planar. On top of the macroscopic curvatures, there is microscopic random roughness on the beam-tube surface. The incident synchrotron radiation will not be only reflected specularly in a single direction, but also scattered in various directions, though certain privileged directions may receive more photons than others.

In this paper, we present results of reflectivity measurements on electroplated copper on stainless steel beam-tubes. The plan of the paper is the following: Section IIA talks about the optical considerations; IIB presents our synchrotron measurements; IIC investigates the absorbtion behaviors; IID offers a brief discussion. Section III concludes our present work.

II. Experiment

A. Optical

As the relativistic protons travel in the bending magnets region with a very large radius, the synchrotron radiation will be directed onto the tube wall surface at grazing incidents. The spectrum of the synchrotron radiation is characterized by

critical energy E_c, with half the total power emitted at energies, $E < E_c$, and peak emission at $E_p = 0.3*E_c$. The 10% and 90% points on the integrated number of photons versus reduced photon energy (E/E_c) curve lie near 0.001 and 1 respectively.[5] In the case of the SSC, E_c = 286 eV with a total flux ~10^{16} photons/meter-second, thus the SR photons with which we are concerned lies mainly between 0.3 eV and 286 eV with $E_p = 0.3*E_c$ = 84 eV. This SR spectrum lies right in a soft X-ray range where the reflecting and absorbing properties are well described by Fresnel theory.[6]

In Fresnel theory, matter is described by a complex dielectric constant, $\varepsilon = \varepsilon_1 + i\varepsilon_2$, or a complex refractive index, $n^* = n + ik$. These four optical constants have been studied extensively for pure metal elements.[7] The dielectric constant and complex refractive index are related by, $\varepsilon = (n^*)^2$, so that either pair of the optical constants is adequate. Given values of either pair, the analytical expression of reflection coefficient for infinite, planar interface between homogeneous, isotropic matter and vacuum (we refer to such an interface below as an ideal surface) exists. For p-polarized light, the reflectivity has the following form:[8]

$$R_f = \left| \frac{\sin\chi - \sqrt{n^{*2} - \cos^2\chi}}{\sin\chi + \sqrt{n^{*2} - \cos^2\chi}} \right|^2 \qquad (1)$$

where χ is the angle of incidence measured from the surface plane. For an ideal surface, all electromagnetic energy incident must be either reflected or absorbed, which means R + A = 1. Scattering via diffused reflection is disallowed.

Unlike ideal surfaces where the reflection and absorption have been studied and known in detail, rough surfaces are not as well understood. There are two methods of approximation which are commonly used. The first one assumes that the surface rms roughness height (σ) is much smaller than the incident wavelength (λ), $\sigma \ll \lambda$. In this case, a perturbation theory from ideal surface solutions is adequate.[9-11] While the second one assumes the opposite, e.g. the surface rms roughness height is much larger than the incident wavelength, $\sigma \gg \lambda$. Although theoretical treatment of the second situation is rather complicated, numerical solutions exist.[12, 13] If the surface roughness height follows Gaussian distribution and the surface roughness profile is smooth (e.g. no sharp bumps or sharp dips),

then the surface roughness can be taken into account in Fresnel formula by including a Debye-Waller type roughness factor:[14, 15]

$$R = R_f \left| e^{-2p_0 p_1 \sigma^2} \right|^2 \qquad (2)$$

where $p_0 = k_0 \sin\chi$, $p_1 = k_0\sqrt{n^{*2} - \cos^2\chi}$, and k_0 is the wave vector of the incident radiation.

B. Measurements

We have utilized the synchrotron radiation source at Brookhaven National Laboratory (BNL) U-16A beam-line to perform our soft X-ray reflectivity measurements. Fig. 1 shows the experimental layout which is enclosed in an Ultra High Vacuum (UHV) chamber with a base pressure of ~8×10^{-10} torr. The incident photons were p-polarized. All the measurements were performed in the plane of the synchrotron.

The photon beam is defined by aperture (A) with a width of 80 μm located 5.7 cm from the sample center. After passing through aperture (A), the beam is directed onto the sample with an angle χ_{in} from the surface. The angle χ_{in} is defined to better than 0.1° by aperture (A) together with apertures located up stream in the beam line. A channeltron detector, which is located on the other side of the surface normal, receives the reflected photons. An aperture (B) with a width of 0.25 mm in the incident plane and an height of 7.5 mm along the out-of-plane direction, located 2.9 cm from the sample, allows only a small portion of the reflected photons to pass through. This enables the detector with the necessary angular resolution in the incident plane direction so that the detector receives only photons with angles around χ_{out}. The angle of incidence, χ_{in}, is varied by rotating the sample. An angular spectrum of the reflected intensity is obtained by scanning the detector in the incident plane. Since we are more concerned about grazing angle incidence than any others, measurements with small incidence angles of χ_{in} are emphasized throughout our experiment. A variety of photon energies have been used in the measurements which ranges from 30 eV (41 nm) to 190 eV (6 nm). By employing the wide aperture in the out-of-plane direction in front of our detector (aperture (B)), we integrate over much of the out-of-plane scattering.

The two samples measured were cut from stainless steel tubes which had been electroplated with Cu. The thickness of the copper is estimated to be on the order of 100 μm. The samples were 5 cm long and 2 cm wide. One sample was mechanically polished after copper electroplating (which we will refer to as the polished sample). The second sample was not polished after copper plating (which we will refer to as unpolished). The minimum grazing angle is limited by the length of a sample and the width of the beam. In our case, the allowed minimum grazing angle is about 1°.

Surface topographies were measured using a Talystep profiling instrument employing a diamond stylus. Although it shows random roughness behavior on all samples both in variation of heights and in horizontal separations, some topographic statistics are observed. For the polished sample, it shows one 1 μm and five 0.4 μm deviations roughly every 2 mm range. For the unpolished sample, it shows five 8.5 μm and fourteen 3 μm deviations every 2 mm.

Fig. 2 displays a series of angular distribution of reflectivities for the polished sample with incident angles around 5° performed with different energies. The inset shows the X-ray beam profile measurement which has a full width half maximum (FWHM) of ~1°. The overall shape of each spectrum is roughly symmetric about its specular direction ($\chi_{out} - \chi_{in} = 0$). All the reflectivities at specular angles for this wide energy range are comparable and close to unity. This indicates that the scattering is predominately in the incident plane with 15° off plane accepting angle included by the aperture (B). We also notice from Fig. 2 that the reflectivity increases from 0.48 to 0.81 as the photon energy decreases from 190 eV to 30 eV.

Fig. 3 displays the corresponding measurement for the unpolished sample. The incident angle is 5° and the photon energy is 190 eV. Although the reflectivity curve still peaks up at specular direction, the value is much smaller than that of the polished sample (~100 times less). The significantly reduced reflectivities in the specular direction implies that in-plane scatterings are no longer dominating. Instead, the reflection is very diffuse. The shape of the spectrum is no longer symmetric. A rapid rise occurs on the small angle side and a long tail occurs on the other side. This might be due to some blocking effect from the surface roughness at small exit angles. It is also interesting to notice that the FWHM (12°) is about one order of magnitude bigger than that of the polished sample (1–2°).

Fig. 4 shows the reflectivity measurement along the specular direction(specular reflectivity) as a function of incident angle for the polished sample at photon energy 120 eV. The theoretical curve calculated from eq. (2) is also shown in the figure. The good agreement is found when the complex refractive index equals $n^* = 0.968 + 0.01i$, while the value for the pure bulk copper is $n^* = 0.968 + 0.054i$.[16] The reason that the measurement favors a smaller value for the imaginary part of the refractive index may be due to the presence of a thin oxidized layer on top of the sample surface. This prediction is consistent with a recent surface composition study for the SSC beam tube material using scanning Auger, which confirms that there is a oxide layer.[17]

Fig. 5 displays the corresponding measurement for the unpolished sample. Although the measurement for the unpolished sample follows the same decreasing trend as the polished sample, the values are only a few tenths of a percent, which are more than two orders of magnitude lower than that of the polished sample. Fresnel calculations using eq. (2) (not shown in the figure) provides much lower values than the measurement.

In Fig. 6, we present the specular reflectivity measurement as a function of the photon energy for the polished sample at a fixed incident beam direction, $\chi_{in} = 2.5°$. Generally speaking, the measurements exhibit a decreasing trend as the photon energy increases. The solid line is the calculation using Fresnel theory. Reasonable agreement with the experiment has been found. The origin of the curve shape will be discussed in Sec. IID.

C. Absorbtion

The aperture we used in front of the channeltron detector is 0.25 mm in width and 7.5 mm in height. It is located 2.9 cm away from the sample (shown in Fig. 1). This configuration allows the detector to accept angles of $\Delta\theta_x=1.0X10^{-2}$ rad (~0.5°) in the incident plane direction and $\Delta\theta_y=0.26$ rad (~15°) along the out of incident plane direction. In another word, our detector allows a best angular resolution of ~0.5° in the incident plane, meanwhile automatically integrates over 15° in the out-of-plane direction. From Fig. 2 we see that the FWHM of the reflectivity angular spectrum for the polished sample is around 1–2°. If we assume the same angular width along the out-of-plane direction, then the opening $\Delta\theta_y$ has

automatically integrated all of the out-of-plane reflection. Therefore, in order to calculate the total reflectivity, we integrate the spectrum in the incident plane and divide by the beam profile integral:

$$\Psi_x = \frac{\int_{-\pi/2}^{\pi/2} \frac{R(\chi)}{\Delta\theta_x} \, d\chi}{\int_{-\pi/2}^{\pi/2} \frac{i(\chi)}{\Delta\theta_x} \, d\chi} \qquad (3)$$

where $R(\chi)$ is the reflectivity angular spectrum, $i(\chi)$ is the beam profile shown in the inset in Fig. 2.

Using this formula, we have calculated the total reflectivity for the spectra shown in Fig. 2 to be 96%, 75%, and 86% for 30 eV, 120 eV, and 190 eV respectively. Or the absorbtions are 4%, 25%, and 14% accordingly.

The situation for the unpolished sample is quite different. From Fig. 3 we notice that the FWHM of the angular spectrum is about 0.21 (12°). It is reasonable to assume that the spectrum is also broad in the out-of-plane direction. In order to calculate the total reflectivity, we have to integrate the spectrum both along the in-plane direction and along the out-of-plane direction. Using eq. 3 we found the integration in the incident plane, Ψ_x, to be 4.6×10^{-2}. The integration along the out-of-plane direction, Ψ_y, requires some assumptions since we do not have detailed measurements in that direction. If we assume the intensity distribution along the out-of-plane direction is Gaussian with the same angular width as in the incident plane, then the distribution along this direction will be proportional to $\exp(-\frac{\chi_y^2}{\delta^2})$, where χ_y is the angle along the out-of-plane direction measured from the incident plane, and $\delta = 0.13$ (FWHM = 0.21). Therefore the total integration along the out-of-plane direction, Ψ_y, is:

$$\Psi_y\left(\frac{\pi}{2}\right) = \int_{-\pi/2}^{\pi/2} \exp\left(-\frac{\chi_y^2}{\delta^2}\right) d\chi_y = \sqrt{\pi}\,\delta\,\mathrm{erf}\left(\frac{\pi}{2\delta}\right) \qquad (4)$$

In our measurements, the aperture (B) along the out-of-plane direction already allows the integration take place from $-\frac{\Delta\theta_y}{2}$ to $\frac{\Delta\theta_y}{2}$, which contributes:

$$\Psi_y\left(\frac{\Delta\theta_y}{2}\right) = \sqrt{\pi}\,\sigma\,\mathrm{erf}\left(\frac{\Delta\theta_y}{2\delta}\right) \tag{5}$$

Therefore, the correction factor (γ) due to the integration over the out of incident plane direction is given by the following:

$$\gamma = \frac{\Psi_y\left(\frac{\pi}{2}\right)}{\Psi_y\left(\frac{\Delta\theta_y}{2}\right)} = \frac{\mathrm{erf}\left(\frac{\pi}{2\delta}\right)}{\mathrm{erf}\left(\frac{\Delta\theta_y}{2\delta}\right)} \tag{6}$$

Plug $\delta = 0.13$ and $\Delta\theta_y = 0.26$ into the above equation, we get $\gamma = \frac{\mathrm{erf}(12.5)}{\mathrm{erf}(1.0)} = 1.2$. The total reflectivity $\Psi_t = \Psi_x * \gamma = 4.6\mathrm{X}10^{-2}*1.2 = 6\%$. This implies that roughly speaking, less then 10% of the incident photons are reflected from the surface and more than 90% are absorbed.

D. Discussion

Although the measured values for the polished and unpolished samples are very different, some trends are common. Fig. 2 & 3 show that the reflectivity spectra peak up at specular directions under all circumstances. Comparing the reflectivities of the unpolished sample (Fig. 3) with the polished (Fig. 2), we see that reductions of two orders of magnitude exist. The significant reduction of reflection and the broad angular span for the unpolished sample indicate the absorbtion is a lot larger for the rough surface and diffused scattering plays important roles. From Figs. 4 and 5 we see the specular reflectivity drops very rapidly as the incident angle increases for both polished and unpolished samples. The best fit complex refractive index for the samples we used are $n^* = 0.968 + 0.01i$ for 120 eV photons, which shifts from pure copper to copper oxides.

The amount of absorbtion is directly related to the surface roughness, which is quite different for the polished and unpolished samples. For the smooth surface,

most of the incident photons (75%–96%) are reflected and only a small portion (4%–25%) is adsorbed in the beam tube material. On the other hand, for the rough surface, only less than 10% of photons are reflected and more than 90% are absorbed. This large difference may be due to the reason that a rough surface can be pictured as being formed by microfacets with different slopes. Although a beam of incident photons shoot on the surface macroscopically with a fixed incident angle, microscopically the incident angle varies on each of the microfacets. The average slope of these microfacets visible to the beam will be higher than that of the macroscopic surface plane. Indeed, the 6% of reflection corresponds to an incident angle of 15°. Subtract the macroscopic incident angle, 5°, we get the average tilting angle of the microfactes from the surface, which is 10°.

The photon reflectivities of beam tube walls are mainly determined by the surface conditions. If the tube wall surfaces are smooth, the radiation will reflect many times before dying off so that a large portion of the wall surface will be illuminated. Consequently, Photon and Electron Stimulated Desorptions (PSD & ESD) will happen all over the place. On the other hand, if the tube wall surfaces are rough, it may only take one reflection to decay the radiation. In this case diffused scattering will be important. In addition, a rough surface has larger surface area and more gas adsorption sites and therefore is harder to clean. There are pro's and con's for either smooth or rough surfaces. In any event, detailed understandings of the reflectivity behaviors are crucial for selecting the optimal tube materials and wall conditions.

The decreasing trend shown in Fig. 6 is worth a discussion. First of all, we would like to speculate for what values of wavelength, surface roughness and angle of incidence will a surface be considered rough. Rayleigh suggested that when photons reflected from surface "peaks" and "valleys" are in phase opposition and cancel, the surface is called rough, which is known as Rayleigh criterion. Stated mathematically, the critical surface roughness $\sigma_c = \frac{\lambda}{8*\sin(\chi_{in})}$.[14] Raleigh criterion is in essence more or less conventional. For 30 eV photons with 2.5° incidence, σ_c is equal to 0.2 μm. Talystep profile measurement for the polished sample tells us that statistically every 2 mm range on the surface, there are five 0.4 μm deviations. Since the surface roughness is comparable to σ_c, the polished surface looks close to a smooth one for the 30 eV photons with 2.5° incidence, where a reflectivity of ~0.9

has been found. As the photon energy increases, σ_c gets smaller and smaller. Consequently, the surface looks rougher and rougher to the incoming photons. This explains why the reflectivity declines in general as the incident photon energy increases.

III. Conclusions

In this paper we presented our efforts on the reflectivity measurements for the next generation accelerator beam tube materials. Our results show that by changing the surface rms roughness height from ~1 μm to ~10 μm, the surface specular reflectivities have been altered by two orders of magnitude. The total reflections for the smooth and rough surfaces are quite different, with ~90% for the smooth one and ~10% for the rough. The small total reflection (or high absorbtion) for the rough surface might be due to the reason that the equivalent incident angle on the microfacets visible to the beam is higher than the macroscopic incident angle. We also notice the refractive indices found from these surfaces are different from the bulk values and shift toward oxide values.

Since the tube wall roughness can be modified to be anywhere a few hundredths of a μm and up, it is important to ask what is the best tube condition for vacuum requirements. To answer this question, we need to perform desorption measurement at the real operation temperatures for a variety of beam tube conditions. The issues must be addressed include: photon and electron desorption coefficients, photoelectron and secondary electron production rates, angular and energy distribution of desorbed species, etc.. A multipurpose UHV system for low temperature measurements, equipped with Kimball Physics Electron Gun, Perkin Elmer X-ray Gun, Quantar Technology 2D-detector, Balzers Quadruple Mass Spectrometer, etc. has been built at the University of Texas at Arlington.

Acknowledgments

We would like to thank Dr. J. Erskine for letting us use his U-16A synchrotron beam and his UHV chamber at Brookhaven National Lab. The work was supported by the SSC lab under contract SSC 91-Z-16301.

References

1. H. T. Edwards, Study on Beam Tube Vacuum with Consideration of Synchrotron Light, Potential Liner Intercept, and Collider Quad/Spool Coil Diameter, (Superconducting Super Collider, Dallas, 1991).
2. A. G. Mathewson, CERN AT/93-11 (1993).
3. P. H. Lippel, Q. T. Jiang, S. P. Erichsrud, A. R. Koymen, and A. H. Weiss, Desorption Induced by Electron Transitions DIET V, Springer Series in Surface Sciences, (Springer-Verlag, Berlin Heidelberg, 1993).
4. A. Maschke, Desorption Induced by Electronic Transitions DIET V, Springer Series in Surface Sciences, (Springer-Verlag, Berlin Heidelberg, 1993).
5. Herman Winick and S. Doniach, Synchrotron Radiation Research, (Plenum Press, New York, 1980).
6. Max Born and Emil Wolf, Principles of Optics, (Pergamon Press, New York, 1965).
7. See any handbook on optical constants such as R. C. Weast and M. J. Astle, CRC Handbook of Chemistry and Physics (CRC Press In. Boca Raton, 1979).
8. See any standard text on electromagnetic theory such as J. A. Stratton, Electromagnetic Theory (McGraw-Hill Book Co., New York, 1941).
9. J. M. Elson, Phy. Rev. B **12**, 2541 (1975).
10. J. M. Elson, Phys. Rev. B **30**, 5460 (1984).
11. E. Kröger and E. Kretschmann, Z. Physik **237**, 1 (1970).
12. C. C. Sung and W. D. Eberhardt, J. Appl. Phys. **49**, 994 (1978).
13. J. A. Holzer and C. C. Sung, J. Appl. Phys. **49**, 1002 (1978).
14. P. Beckmann and A. Spizzichino, The scattering of electromagnetic waves from rough surfaces, (Pergamon Press, New York, 1963).
15. S. C. Woronick, Ph.D. disetaion, (State University of New York at Stony Brook, 1990).
16. Edward D. Palik, Handbook of Optical Constants of Solids, (Academic Press, Inc., New York, 1985).
17. A. Koymen and et al, unpublished.

Figure Captions

Fig. 1 Experimental layout for reflectivity measurements. Apertures A & B are located in front of the light source and detector respectively.

Fig. 2 Angular distribution of reflectivities for the polished sample with incident angles around 5° performed at different energies. Spectra peak up at specular angles with roughly symmetric shapes. The FWHMs are around 1–2°. The values of specular reflectivities are comparable to unity. Note inset illustrates the beam profile, where the values have been normalized to the maximum.

Fig. 3 Angular distribution of reflectivities for the unpolished sample with incident angle of 5° performed with 190 eV beam. Although spectra still peak up at specular direction, the shape is no longer symmetric. The value is more than two orders of magnitude smaller than the polished sample.

Fig. 4 Specular reflectivity as a function of incident angle for the polished sample, measured at photon energy 120 eV. Good agreement has been found with calculations from Fresnel theory (shown as the solid line).

Fig. 5 Specular reflectivity as a function of incident angle for the unpolished sample, measured at photon energy 120 eV. Values are more than two orders of magnitude smaller than the polished.

Fig. 6 Specular reflectivity as a function of the photon energy for the polished sample at a fixed incident beam direction, $\chi_{in} = 2.5°$. The value decreases as the photon energy increases. It shows reasonable agreement with calculations using Fresnel theory (solid line).

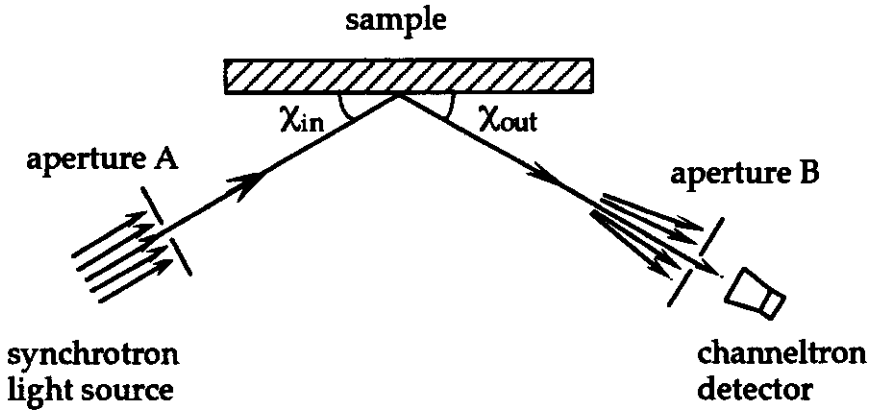
sample
χ_{in}
χ_{out}
aperture A
aperture B
synchrotron
light source
channeltron
detector

Fig. 1

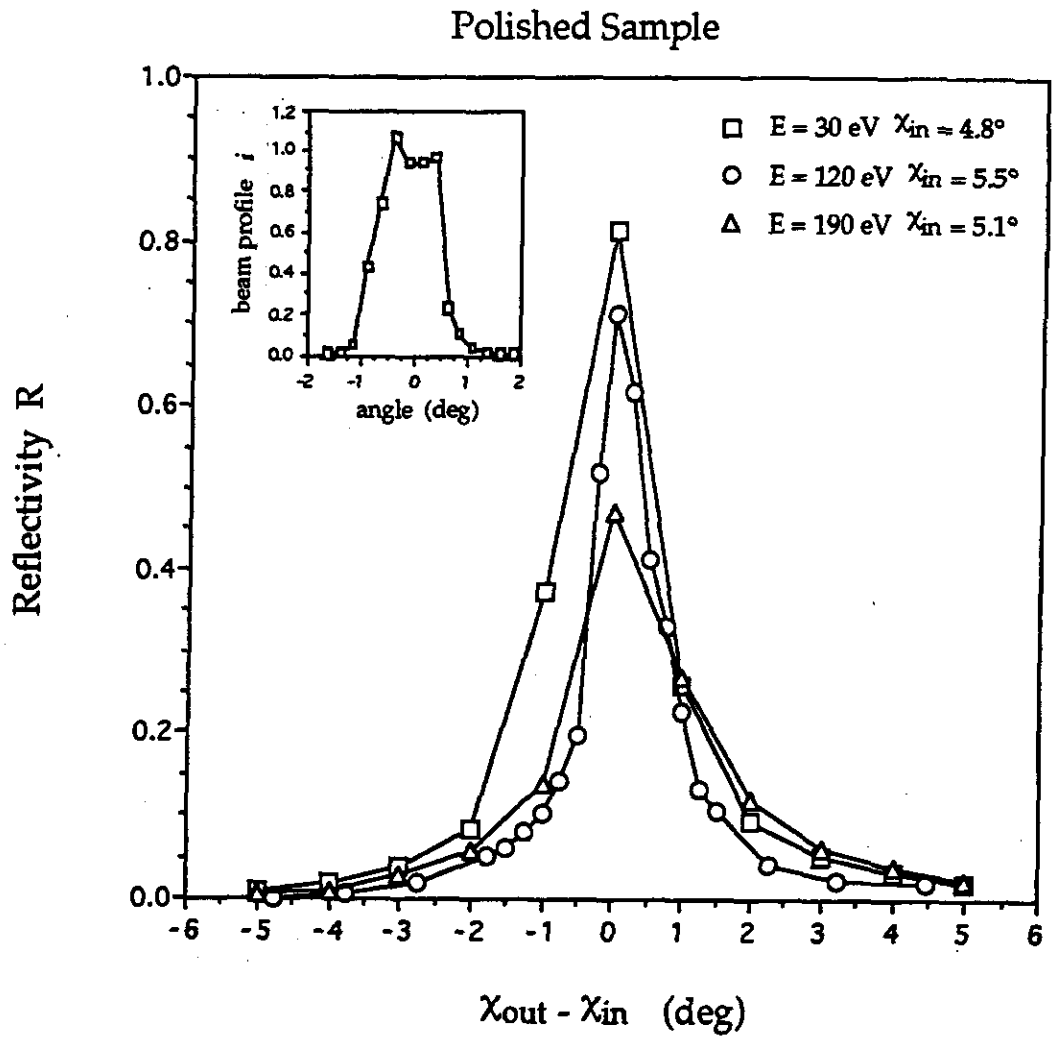
Polished Sample
Reflectivity R
χout - χin (deg)
E = 30 eV χin = 4.8°
E = 120 eV χin = 5.5°
E = 190 eV χin = 5.1°
beam profile i
angle (deg)

Fig. 2

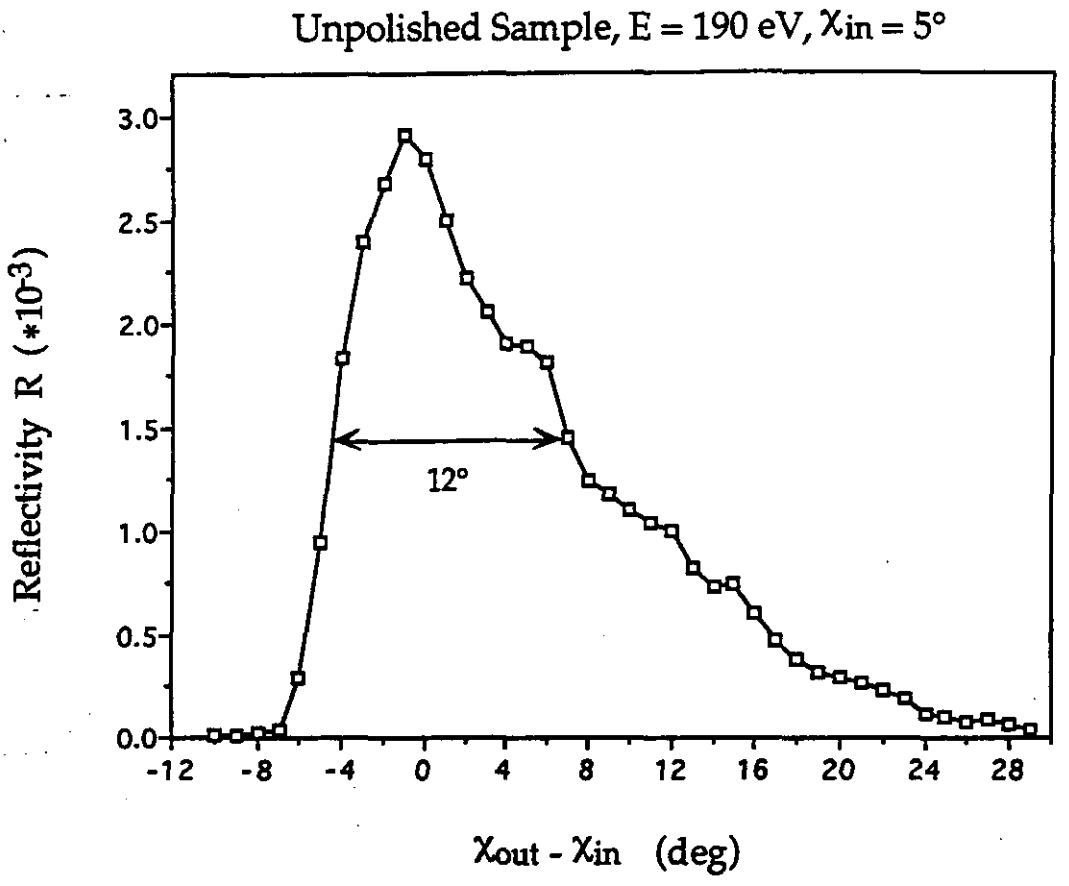
Unpolished Sample, E = 190 eV, χin = 5°
Reflectivity R (*10-3)
3.0
2.5
2.0
1.5
1.0
0.5
0.0
12°
-12
-8
-4
0
4
8
12
16
20
24
28
χout - χin (deg)

Fig. 3

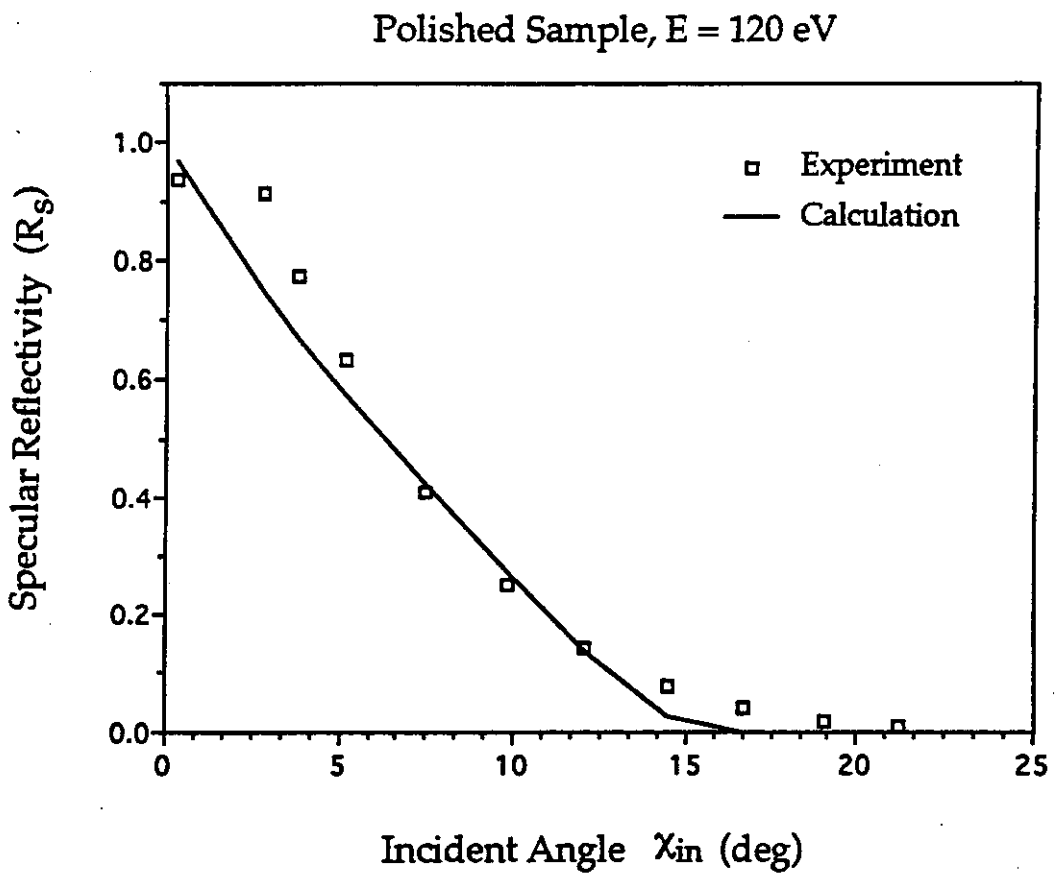
Polished Sample, E = 120 eV
Experiment
Calculation
Specular Reflectivity (R_S)
1.0
0.8
0.6
0.4
0.2
0.0
0
5
10
15
20
25
Incident Angle χ_{in} (deg)

Fig. 4

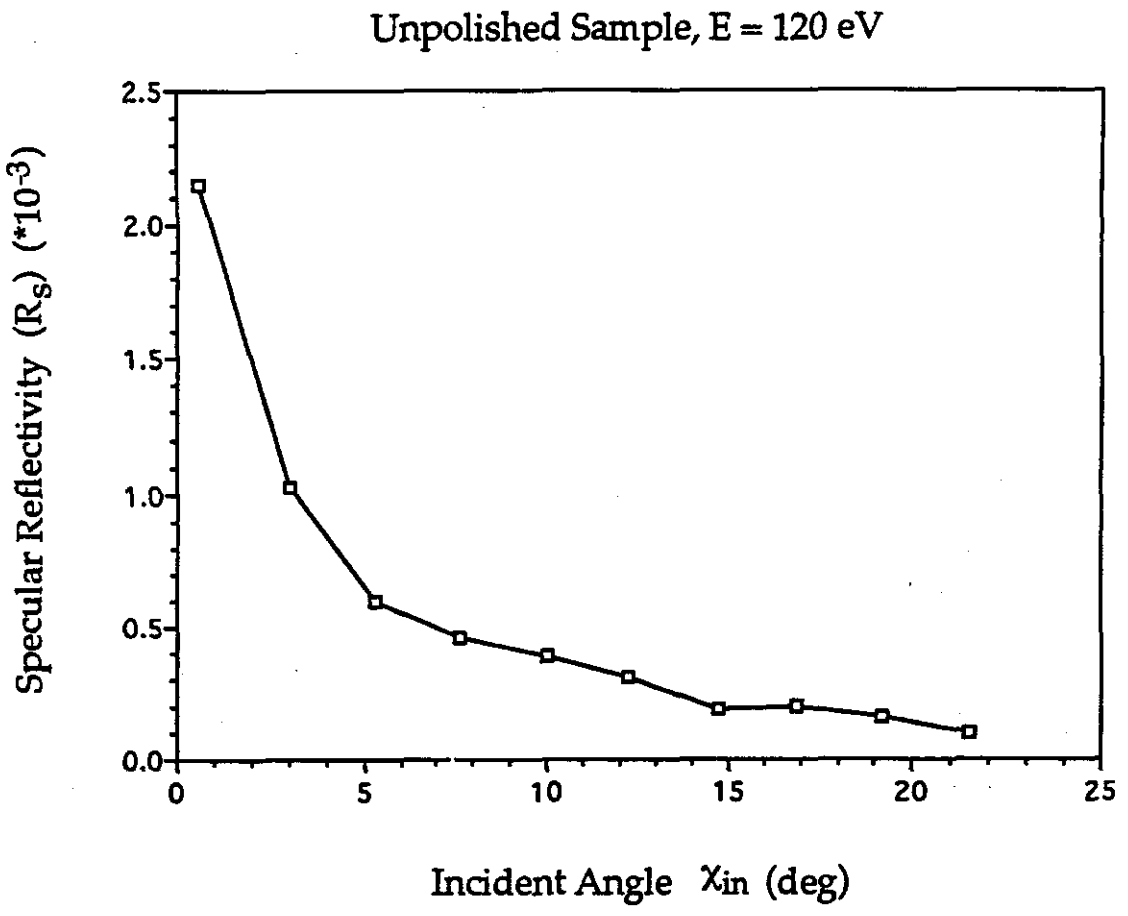
Unpolished Sample, E = 120 eV
Specular Reflectivity (R_s) (*10^{-3})
2.5
2.0
1.5
1.0
0.5
0.0
0
5
10
15
20
25
Incident Angle χ_{in} (deg)

Fig. 5

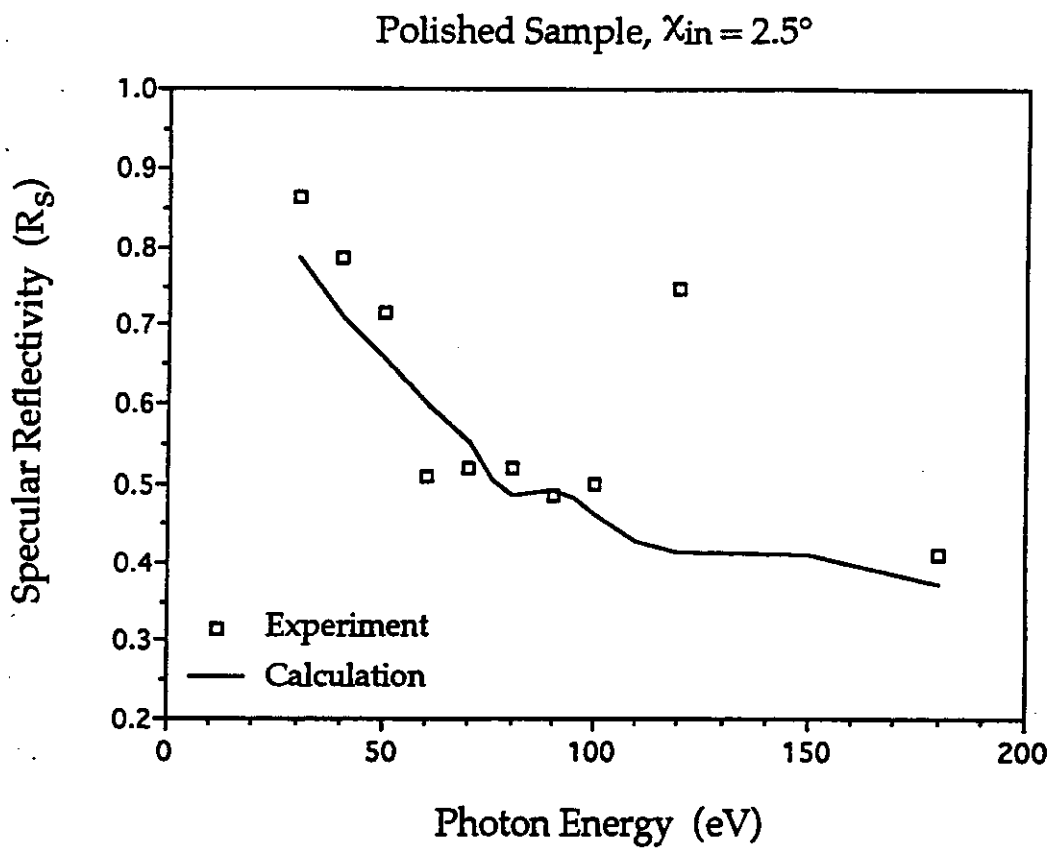
Polished Sample, $\chi_{in} = 2.5°$
Specular Reflectivity (R_S)
1.0
0.9
0.8
0.7
0.6
0.5
0.4
0.3
0.2
0
50
100
150
200
Experiment
Calculation
Photon Energy (eV)

Fig. 6